Molecular plasticity regulates oligomerization and cytotoxicity of the multi-peptide length Aβ pool

Annelies Vandersteen[1,2,3,4], Marcelo Fabricio Masman[5,6], Greet De Baets[1,2,3], Wim Jonckheere[1,3], Kees van der Werf[4], Siewert Jan Marrink[6], Jef Rozenski[7], Iryna Benilova[8], Bart De Strooper[8], Vinod Subramaniam[4], Joost Schymkowitz[1,2], Frederic Rousseau[1,2], and Kerensa Broersen[3,4*]

[1] Switch Laboratory, Flanders Institute for Biotechnology (VIB), B-3000 Leuven, Belgium
[2] Department of Molecular Cell Biology, K.U. Leuven, B-3000 Leuven, Belgium
[3] Structural Biology, Flanders Institute for Biotechnology (VIB) and Vrije Universiteit Brussel (VUB), B-1050 Brussels, Belgium
[4] Nanobiophysics group, MIRA Institute for Biomedical Technology and Technical Medicine and MESA+ Institute for Nanotechnology, University of Twente, 7500 AE Enschede, The Netherlands
[5] Department of Molecular Neurobiology, University of Groningen, 9747 AG Groningen, The Netherlands
[6] Groningen Biomolecular Sciences and Biotechnology Institute and Zernike Institute for Advanced Materials, University of Groningen, 9747 AG Groningen, The Netherlands
[7] Laboratory of Medicinal Chemistry, Rega Institute for Medical Research, B-3000 Leuven, Belgium
[8] VIB Center for Biology of Disease, Flanders Institute for Biotechnology (VIB) and Center for Human Genetics, K.U. Leuven, B-3000 Leuven, Belgium

Running title: *Molecular plasticity determines Aβ length toxicity*

To whom correspondence should be addressed: Kerensa Broersen, Faculty of Science and Technology, Nanobiophysics, MIRA Institute for Biomedical Technology and Technical Medicine, University of Twente, Enschede, The Netherlands. Tel: +31(0)534893655, Fax: +31(0)534891105, e-mail: k.broersen@utwente.nl

Background: Aβ peptide, implicated in Alzheimer disease, occurs in various lengths.
Results: Non-abundant $Aβ_{1-38}$ and $Aβ_{1-43}$ affect oligomerization, cytotoxicity and aggregation of $Aβ_{1-40}$ and $Aβ_{1-42}$.
Conclusion: Small amounts of Aβ lengths other than $Aβ_{1-40}$ or $Aβ_{1-42}$ significantly alter the behavior of the total Aβ pool.
Significance: Drug strategies targeting APP processing to affect $Aβ_{1-38}$ levels need careful consideration.

SUMMARY
    Current therapeutic approaches under development for Alzheimer disease, including γ-secretase modulating therapy, aim at increasing the production of $Aβ_{1-38}$ and $Aβ_{1-40}$ at the cost of longer Aβ peptides. Here, we consider the aggregation of $Aβ_{1-38}$ and $Aβ_{1-43}$ in addition to $Aβ_{1-40}$ and $Aβ_{1-42}$; in particular their behavior in mixtures representing the complex *in vivo* Aβ pool. We demonstrate that $Aβ_{1-38}$ and $Aβ_{1-43}$ aggregate similar to $Aβ_{1-40}$ and $Aβ_{1-42}$, respectively, but display variation in kinetics of assembly and toxicity due to differences in short timescale conformational plasticity. In biologically relevant mixtures of Aβ, $Aβ_{1-38}$ and $Aβ_{1-43}$ significantly affect the behaviors of $Aβ_{1-40}$ and $Aβ_{1-42}$. The short timescale conformational flexibility of $Aβ_{1-38}$ is suggested to be responsible for enhancing toxicity of $Aβ_{1-40}$ whilst exerting a cyto-protective effect on $Aβ_{1-42}$. Our results indicate that the complex *in vivo* Aβ peptide array, and variations thereof, is critical in Alzheimer disease, which can influence the selection of current and new therapeutic strategies.

    Extracellular deposits containing the amyloid-β peptide (Aβ) represent one of the hallmarks of Alzheimer disease (AD) (1). Aβ is generated from

1

the transmembrane amyloid precursor protein (APP) by β- and γ-secretase-mediated cleavage (2-4). This action primarily results in the production of the 40-amino acid $A\beta_{1-40}$ peptide and smaller amounts of the 42-amino acid $A\beta_{1-42}$ peptide, in addition to minute quantities of other Aβ peptides ranging in length from 27 to 43 amino acids (5,6). The observed variation at the Aβ carboxy terminus is a consequence of the heterogeneous γ-secretase processing pattern (7) that first generates $A\beta_{1-48}$ and $A\beta_{1-49}$ peptides through cleavage of APP at the ε-site followed by successive trimming of every three to four residues (8,9). Hence, the preferential $A\beta_{1-40}$ production pathway involves the intermediate formation of $A\beta_{1-43}$, $A\beta_{1-46}$, and $A\beta_{1-49}$ (10). The array of Aβ peptides that is produced in this way can be affected by clinical mutations in APP (8,11) or in the presenilin-1 (PS1) active site subunit of the γ-secretase complex (8,11,12). Mutations of PS1 potently shift the ε-cleavage site on APP towards the $A\beta_{1-38}$ production pathway with intermediate formation of $A\beta_{1-42}$, $A\beta_{1-45}$, and $A\beta_{1-48}$ (10).

Generally, longer Aβ peptides are more hydrophobic as the carboxy-termini progressively form part of the transmembrane domain of APP and are therefore considered more aggregation prone (13-15). Consistent with this finding, senile plaques have been found to be primarily composed of $A\beta_{1-42}$ and $A\beta_{1-43}$ while shorter Aβ peptides remain largely undetected (16-18). Based on these observations, γ-secretase inhibitors (GSIs) were developed that aimed at lowering the activity of γ-secretase and reducing Aβ production. However, the multifunctionality of the γ-secretase enzyme, including a critical role in the Notch signaling process, led to the recognition that total inhibition of this enzyme is un undesired approach. This observation served as a starting point for the generation of γ-secretase modulators (GSMs). which fine-tune the action of γ-secretase to shift the production of Aβ peptides towards shorter variants while leaving the total Aβ peptide production and activity of γ-secretase unchanged (19,20). Given the finding that specifically aggregated Aβ peptide can lead to a neurotoxic response, GSMs offered in this way a promising perspective as a potential agent to slow down the progress of senile plaque deposition in AD by decreasing the production of $A\beta_{1-42}$ whilst increasing that of $A\beta_{1-38}$. The first generation of

GSMs were classified as non-steroidal anti-inflammatory drugs (NSAIDs) and derivatives thereof. Administration of these drugs to healthy individuals showed positive effects on cognitive function which could be entirely attributed to the cyclo-oxygenase (COX) inhibitory action of the compound without displaying GSM action (21,22). Clinical trials with non-COX inhibitory NSAIDs did not display protective effects on AD disease progress possibly as a result of the low potency and poor brain penetrance of the compounds, inhibition of Notch processing or accumulation of APP C-terminal fragments (23). A next generation of Notch sparing GSMs and non-NSAID derived compounds with improved potency and brain penetration are currently being developed but yet await clinical trials (22).

The reported neurotoxicity of $A\beta_{1-43}$ (12) as well as the observed increasing (24) and decreasing $A\beta_{1-38}$ (25) levels in CSF upon AD progress, indicate that the contributions of $A\beta_{1-38}$ and $A\beta_{1-43}$ to AD progression require further elucidation. By comparing their pathogenicity, aggregation profiles and biophysical properties with that of well-studied $A\beta_{1-40}$ and $A\beta_{1-42}$ we show that $A\beta_{1-38}$ and $A\beta_{1-43}$ both form aggregates which differ in cytotoxic potential. We further show that inclusion of $A\beta_{1-38}$ and $A\beta_{1-43}$ into complex mixtures containing $A\beta_{1-40}$ and $A\beta_{1-42}$ substantially affects the behavior of total Aβ and that $A\beta_{1-38}$ and $A\beta_{1-40}$, previously considered non-amyloidogenic, can unexpectedly become toxic in these mixtures. These findings have been related to conformational plasticity of the respective peptides and highlight the relevance of understanding the role of carboxy-terminal variation of Aβ peptides and their potential as therapeutic targets.

EXPERIMENTAL PROCEDURES

Preparation of Aβ peptides and peptide ratios - Aβ peptides (rPeptide) were dissolved, and mixed as described before (26,27). Briefly, Aβ was dissolved into 1,1,1,3,3,3-hexafluor-2-propanol (HFIP), evaporated with a N_2 stream and redissolved in dimethyl sulfoxide (DMSO). Solvents were removed by elution over a 5 mL HiTrap desalting column (GE Healthcare) into a 50 mM Tris buffer pH 7.4 containing 1 mM EDTA. Peptide concentrations were measured using the Coomassie (Bradford) Protein Assay kit

(Thermo Scientific) against a bovine serum albumin standard (Thermo Scientific). Aβ peptide concentrations were diluted to a concentration of 50 μM in 50 mM Tris buffer pH 7.4 containing 1 mM EDTA and incubated at 25 °C under quiescent conditions for further experiments.

Thioflavin T fluorescence - Fibrillation kinetics of Aβ in the presence of 12 μM thioflavin T (ThT) were followed *in situ* at 25 °C using a Fluostar OPTIMA fluorescence plate reader (BMG LABTECH GmbH, Germany) at an excitation wavelength of 440 nm and an emission wavelength of 480 nm. Readings were recorded in triplicate every 5 min for a period of 10 h and corrected by subtracting the intensity obtained for buffer containing 12 μM ThT. The end of the lag phase was determined manually. Elongation rate was fitted to the central region of the exponential phase. Final fluorescence was determined at 10 h of incubation.

Dot blot - At various time points a volume of 5 μL sample was spotted onto Protran BA85 nitrocellulose blotting membrane (Whatman). The membranes were blocked at 25 °C in phosphate-buffered saline containing 0.2 % Tween20 (PBST XL) for 1 h and incubated for 1 h at 25 °C with primary rabbit polyclonal anti-oligomer antibody (A11) (Invitrogen), diluted 1:4000 in 100 mM Hepes pH 7.0 (28). After incubation with secondary anti-rabbit-HRP-tagged antibody (Promega), diluted 1:5000 in phosphate-buffered saline containing 0.05 % Tween20 (PBST) for 0.5 h at 25 °C, the membranes were visualized using the Immobilon™ Western chemiluminescent HRP substrate system (Millipore, USA).

Transmission electron microscopy (TEM) - A volume of 5 μL of Aβ was adsorbed to carbon-coated FormVar film on 400-mesh copper grids (Agar Scientific Ltd) for 1 min. The grids were washed in ultrapure water (Merck) and stained with 1 % (wt/vol) uranyl acetate (VWR). Samples were studied using a JEOL JEM-2100 microscope at an accelerating voltage of 200 kV or a JEOL JEM-1400 microscope at an accelerating voltage of 80 kV (JEOL Ltd., Japan).

Atomic force microscopy (AFM) - AFM imaging was performed on a custom built instrument using Si_3N_4 tips (Veeco Instruments, Woodbury NY, USA, type MSCT-AUHW) with a spring constant of 0.5 N/m and a nominal tip radius of 10 nm. The measurements were made in tapping mode in air, with a tapping amplitude of less than 4 nm. The AFM scan settings were optimized to minimum force interaction with the sample. AFM samples were prepared by placing 5 μL of sample on freshly cleaved mica. After 4 min adsorption time, unbound Aβ was washed off with twice 100 μL ultrapure water (Merck) and dried using a gentle N_2 stream. The images are represented in 3D after removal of height discontinuities between subsequent scan lines and compensation for piezo drift using SPIP software (Image Metrology A/S, Lyngby, Denmark).

Far-UV circular dichroism (CD) - After 1.5 h incubation Aβ was diluted to 15 μM and placed in a quartz cuvette with an optical path of 3 mm and far-UV circular dichroism spectra were recorded in a Jasco J-715 spectrometer. The wavelength range was set from 260 to 190 nm with 0.2 nm resolution, 2.0 s response time, 2.0 nm bandwidth at a scanning speed of 50 nm/min. Data were collected as averages of eight scans. The spectra obtained were corrected by subtracting the spectrum obtained for buffer only.

Attenuated total reflection fourier-transform infrared spectroscopy (ATR FT-IR) - Using a Bruker Tensor 27 infrared spectrophotometer equipped with a Bio-ATR II accessory, infrared spectra of aggregating Aβ (220 μM, 25 °C, in 50 mM Tris buffer pH 7.4 containing 1 mM EDTA) were recorded. The samples were applied to the FT-IR sample holder and incubated for 1.5 h. Spectra were recorded in the range of 900 to 3500 cm^{-1} at a spectral resolution of 4 cm^{-1} at the beginning (time 0) and the end (time 1.5 h) of the experiment. Each measurement consisted of 120 accumulations. The spectrophotometer was continuously purged with dried air. The obtained spectra were corrected for atmospheric interference, baseline-subtracted and rescaled in the amide I area (1700 to 1600 cm^{-1}). Changes of secondary structure over 1.5 h incubation were analyzed by subtraction of the spectrum recorded at time 0.

In silico predictions - The statistical mechanics algorithm TANGO (29) was used to predict aggregation-prone regions in the Aβ peptide sequence (30). TANGO provides an aggregation propensity (0-100 %) per residue as output. An aggregating region is defined as a continuous stretch of residues with an individual TANGO

score higher than 5 % and a total score for the region higher than 50 %. Total TANGO scores are calculated as the sum of the individual residual TANGO scores for a given sequence. TANGO calculations were performed using http://tango.switchlab.org/ at a pH of 7.0, a temperature of 298.15 K and 0.02 M ionic strength without N- or C- terminal protection.

Molecular dynamics (MD) simulations - The NMR structure (protein data bank entry 1IYT) was used as starting structure of $A\beta_{1-42}$ and as a template to generate the other Aβ species studied here. All MD simulations were performed with GROMACS 4.5.3, using the OPLS/AA force field (31). Experimental details are described in SI. The LINCS algorithm (32) was used for bond-length constraining. The non-bonded pair list was updated every 10 fs. The simulation of each system was repeated at least 10 times, and then individually analyzed and their averaged properties here reported. Programs included in the GROMACS package, as well as some in-house scripts were used to perform the analysis of the trajectories. Molecular graphics images were produced using the UCSF Chimera package from the Resource for Biocomputing, Visualization, and Informatics at the University of California, San Francisco (supported by NIH P41 RR001081) (33).

Neuroblastoma cells and cytotoxicity - All tissue culture reagents were obtained from Gibco, Life Technologies. The human neuroblastoma cell line SH-SY5Y (ATCC number CRL-2266) was cultured in D-MEM:F-12 supplemented with 10 % fetal bovine serum (HyClone, ThermoScientific). The cells were incubated at 37 °C in a humidified 5 % CO_2 atmosphere. Cytotoxicity assays were performed in 96-well plates after plating 25,000 cells per well in serum-deprived D-MEM:F-12. After pre-aggregation for 1.5 h Aβ was diluted in D-MEM:F-12 and added to the cells. After 24 h treatment, cell viability was analyzed using the Cell Titer Blue Cell Viability assay (Promega). After 4 h, color conversion was analyzed by measuring the fluorescence intensity of the samples at an excitation wavelength of 544 nm and an emission wavelength of 590 nm using a Fluostar OPTIMA fluorescence plate reader. Values are percent of cell viability ± SD, buffer signal was normalized to 100 %.

Statistical analysis - Results from ThT fluorescence and cytotoxicity experiments were analyzed using two-tailed unpaired t-test for significance. Significance is indicated by *** $P<0.0001$, ** $P<0.0005$, and * $P<0.005$. MD results were analyzed using two-way ANOVA with repeated measures to determine whether each group differs significantly from each other, and multivariate analysis to determine at which specific point the groups significantly differed. Bonferroni *post-hoc* analysis was applied. Significance is indicated by ## $P<0.005$. All properties determined by MD techniques are reported as the average property of 10 simulations ± SEM.

RESULTS

Aβ peptide length determines aggregation, oligomerization and toxicity - It has been reported before that $A\beta_{1-40}$ and $A\beta_{1-42}$ display different aggregation kinetics (13,34). Consistent with these data, we also observed substantial differences in aggregation kinetics as a function of peptide length (Fig. 1A) when comparing $A\beta_{1-38}$, $A\beta_{1-40}$, $A\beta_{1-42}$ and $A\beta_{1-43}$ using thioflavin T (ThT) fluorescence. While $A\beta_{1-38}$ and $A\beta_{1-40}$ showed a delayed onset of aggregation, $A\beta_{1-42}$ and $A\beta_{1-43}$ rapidly aggregated as suggested by the immediate rise in ThT fluorescence signal. Even though the aggregation regimes of $A\beta_{1-38}$ and $A\beta_{1-40}$ are generally alike with a distinct lag phase and significant and sigmoidal development of ThT signal after 10 h of incubation, $A\beta_{1-38}$ showed a more rapid onset of aggregation compared to $A\beta_{1-40}$. The final (10 h) ThT fluorescence intensity of both $A\beta_{1-42}$ and $A\beta_{1-43}$ aggregates was very low compared to $A\beta_{1-38}$ and $A\beta_{1-40}$ (Fig. 1B) and has been reported to correlate with the weight concentration and the morphology of the formed fibrils (35). Transmission electron microscopy (TEM) showed that 0.5 h of incubation of $A\beta_{1-42}$ and $A\beta_{1-43}$ resulted in networks of intertwined fibrils while for $A\beta_{1-38}$ and $A\beta_{1-40}$ aggregates were absent (Fig. 1C). Upon incubation for 4 h the fibrillar network observed for $A\beta_{1-43}$ had progressed into polymorphous clusters interconnected by mature fibrils. $A\beta_{1-42}$ showed a similar organization yet short and aligned fibrils seemed more prevalent compared to $A\beta_{1-43}$. In contrast, $A\beta_{1-38}$ and $A\beta_{1-40}$ both formed long, negatively stained and regularly twisted fibrils

4

with a diameter of 8-12 nm which is typically observed for amyloid-like fibrils (36). All Aβ peptides formed extensive fibrillar networks upon incubation for 24 h. To establish by which mechanism carboxy-terminal variation affected the observed aggregation characteristics of Aβ, the statistical thermodynamics algorithm TANGO was used to predict aggregating stretches in the various Aβ peptides tested. TANGO scores further showed that, in general, increasing aggregation propensity could be observed with increasing peptide length with the exception of Aβ varying in length from 37 to 40 amino acids (Fig. 1D). A per-residue analysis of the aggregation propensity showed that all Aβ sequences contain a common aggregating stretch ranging from residue 16 to residue 22 (37) (Fig. 1E). A second aggregating region starts at residue 28 and spans the remaining carboxy-terminal part of the sequence and showed strong variation with Aβ length, owing predominantly to the presence of two subsequent glycine residues, which disfavor aggregation but which are compensated by additional aggregation promoting residues in the longer forms. Our analysis shows that differences in aggregation propensity directly stem from C-terminal variation. In line with our observation that $A\beta_{1-38}$ aggregates faster than $A\beta_{1-40}$ (Fig. 1A), TANGO predicted a slightly higher aggregation propensity for $A\beta_{1-38}$ than for $A\beta_{1-40}$ (Fig. 1D,E).

ThT does not interact strongly with oligomeric Aβ (38) while soluble oligomeric Aβ is generally considered to represent the toxic species (39-41). We used complementary oligomer-sensitive techniques such as the A11 oligomer-specific antibody (28) and atomic force microscopy (AFM) to obtain information on the lifetime of oligomeric Aβ as a function of C-terminal variation. Aβ peptides were allowed to aggregate and were tested for A11-reactivity at various time points of incubation (Fig. 2A). $A\beta_{1-42}$ and $A\beta_{1-43}$ formed A11-positive oligomers already after 0.5 h of incubation while $A\beta_{1-38}$ and $A\beta_{1-40}$ only interacted with the A11-antibody after an incubation time of 5 and 6 h, respectively, with $A\beta_{1-38}$ exhibiting substantially stronger staining with the antibody than $A\beta_{1-40}$. Complementary to A11 reactivity, AFM imaging of samples upon 1.5 h of incubation showed the presence of small oligomeric species for all Aβ peptides tested, including $A\beta_{1-38}$ and $A\beta_{1-40}$ (Fig. 2B). Even though oligomers were

present for all Aβ peptides tested, $A\beta_{1-38}$ and $A\beta_{1-40}$ oligomers only developed into A11-positive oligomers at a later stage compared to $A\beta_{1-42}$ and $A\beta_{1-43}$. Cytotoxicity of oligomeric Aβ upon carboxy-terminal variation was assessed using neuroblastoma cell line SH-SY5Y (Fig. 2C). A11-positive oligomers derived from $A\beta_{1-42}$ and $A\beta_{1-43}$ induced loss of cell viability at a concentration of 5 μM while those derived of $A\beta_{1-38}$ and $A\beta_{1-40}$ affected cell viability only at a significantly higher concentration of 20 μM.

Aβ lengths display conformational differences - Circular dichroism (CD) and fourier transform infrared (FT-IR) spectroscopy were used to evaluate Aβ structure after 1.5 h of incubation. The spectra recorded for $A\beta_{1-38}$ and $A\beta_{1-40}$ using CD were very similar, and displayed typical characteristics of a largely unstructured protein while the spectra of $A\beta_{1-42}$ and $A\beta_{1-43}$ showed pronounced β-sheet formation with a minimum intensity at a wavelength of 218 nm (Fig. 3A). As FT-IR is more sensitive to β-sheet formation than CD and can distinguish between parallel and anti-parallel β-sheet arrangements, FT-IR measurements were performed complementary to CD. Figure 3B shows difference spectra obtained by subtraction of the spectrum of non-aggregated Aβ (time 0) from the spectrum recorded after 1.5 h of incubation. The strong increase of absorbance at a wavelength of 1627 cm^{-1} concurrent with a loss of signal between 1650-1655 cm^{-1} and 1680 cm^{-1} for all four peptides tested, indicated that β-sheet formation took place during the 1.5 h incubation time at the cost of random coil and β-turn structure. The more narrow peak for $A\beta_{1-38}$ suggests the formation of a more stable β-sheet as a result of more extensive H-bonding, compared to the other peptide lengths investigated although $A\beta_{1-40}$ was found to form most β-sheet judging from a higher signal intensity at a wavelength of 1627 cm^{-1}. The small increase at 1695 cm^{-1} seen here for $A\beta_{1-38}$ and $A\beta_{1-43}$ in addition to the increase at a wavelength of 1627 cm^{-1} reveals the formation of an antiparallel oriented β-sheet which has been typically used as a fingerprint for oligomer formation (42). Variation in evolution of these regions is observed between the Aβ isoforms. This observation suggests that the various Aβ isoforms display small structural differences during aggregation. Even though CD and FT-IR provide useful structural information in

terms of an average of the entire protein sequence, they do not provide insight into the behavior of individual residues in the sequence, and, hence, are not able to address the question why the addition of two valines in $A\beta_{1-40}$ rendered this peptide less aggregation prone than $A\beta_{1-38}$. Also CD and FT-IR spectroscopy were unable to report on short-time scale conformational flexibility of peptides potentially required to trigger the onset of aggregation. We used molecular dynamics (MD) simulations to establish whether individual residues contributed to changes in peptide conformation which could explain the observed results. We focused our observations on definition of secondary structure of proteins (DSSP) analysis (43). Here, we report the DSSP results as: coil (unstructured conformation), extended conformation (β-bridge plus β-sheet structures), loop (bend plus turns), and helical conformation (α-helix plus 3_{10}-helix plus π-helix). All peptides presented a general trend to possess a mixture of a collapsed coil structure and helical conformation for residues 1-20. N-terminal helical structure was partially retained over time, whereas C-terminal helicity, if any, was rapidly lost (Supplementary Fig. 1). Also as a general observation, all extended conformations occurred between residues 21-28 and residues 32 to the C-terminal amino acid. A loop section comprising residues 29-31 formed flexible links between these extended portions. Contrary to what was expected, $A\beta_{1-38}$ conformation behavior most closely resembled that of $A\beta_{1-42}$, rather than $A\beta_{1-40}$ (Fig. 4A,B, Supplementary Fig. 1). Over the 100 ns time scale of the simulations, $A\beta_{1-38}$ showed a marked tendency to form extended conformations (Fig. 4A,B), comparable to $A\beta_{1-42}$ and $A\beta_{1-43}$ (Fig. 4B, B1). $A\beta_{1-40}$, on the other hand, exhibited low tendency to form extended conformations (Fig. 4A). Interestingly, during the first tens of nanoseconds the behavior of $A\beta_{1-38}$ was erratic and fluctuated between resembling $A\beta_{1-40}$ and $A\beta_{1-42}/A\beta_{1-43}$. Only after 50 ns of simulation the content of extended conformation invariably increased (Fig. 4A,D). $A\beta_{1-42}$ and $A\beta_{1-43}$ seemed to accumulate and stabilize better their extended conformations, from earlier simulation times onwards (Fig 4B,B1, Supplementary Fig. 2). The same behavior was reflected in the overall helicity of the peptides (Fig. 4C) revealing a slight, yet statistically significant, higher tendency to retain

its helical conformation for $A\beta_{1-38}$ in comparison to $A\beta_{1-42}$ and $A\beta_{1-43}$. A marked increase in the helicity of residues 20-23 and 28 was uniquely observed for $A\beta_{1-40}$ (Fig. 4C,D). Collectively, these data showed that the behaviors of $A\beta_{1-42}$ and $A\beta_{1-43}$ were remarkably similar in terms of their high tendency to form an extended β-sheet conformation while $A\beta_{1-40}$ retained helicity longer. The $A\beta_{1-38}$ peptide showed very interesting behavior in terms of its highly fluctuating tendency to form extended β-sheet conformation. Over time $A\beta_{1-38}$ conformation alternated rapidly between $A\beta_{1-42}/A\beta_{1-43}$-like conformation and $A\beta_{1-40}$-like conformation before forming stable, extended β-sheet.

Mixtures of Aβ show complex aggregation behavior - To evaluate the influence of the observed differences between Aβ isoforms in a more biologically relevant setting, we mimicked the complex pool of various Aβ peptide lengths as observed in *vivo* by preparing Aβ peptide mixtures containing $A\beta_{1-40}$, or $A\beta_{1-42}$ and $A\beta_{1-38}$, or $A\beta_{1-43}$. Increased levels of $A\beta_{1-38}$ in the CSF of AD patients are reported (24), as well as an increased generation of this peptide due to PS-1 mutations (44). Some forms of familial AD display increased generation of $A\beta_{1-43}$ (44), a peptide length frequently present in amyloid plaques (18). $A\beta_{1-40}$ and $A\beta_{1-43}$ were shown to directly interact using ESI-MS (Supplementary Fig. 4C) although these dimeric species only accumulated at a population of ~1 % (Supplementary Fig. 3C). Effective but low accumulation of mixed dimers was also observed upon mixing $A\beta_{1-38}$ and $A\beta_{1-42}$ (Supplementary Fig. 3B,4B). Mixed dimeric complex formation was further detected for $A\beta_{1-38}$:$A\beta_{1-40}$ and $A\beta_{1-42}$:$A\beta_{1-43}$ (Supplementary Fig. 3,4). Along the lines of the earlier identified processing pathways of APP toward the formation of either $A\beta_{1-40}$ and $A\beta_{1-38}$ with $A\beta_{1-43}$ and $A\beta_{1-42}$ as intermediates, respectively (10), we mapped dose-response curves of the presence of $A\beta_{1-43}$ and $A\beta_{1-38}$ on the aggregation kinetics of $A\beta_{1-40}$ and $A\beta_{1-42}$, respectively, using ThT fluorescence (Fig. 5). We reported earlier that $A\beta_{1-42}$:$A\beta_{1-40}$ mixtures behave differently according to their proportional presence (26). Titration of $A\beta_{1-40}$ with increasing concentrations of $A\beta_{1-43}$ substantially reduced the lag phase of aggregation to become similar to that of $A\beta_{1-43}$ alone while final fluorescence intensities were not affected (Fig. 5A,C). These observations

6

suggest that $A\beta_{1-43}$ dominantly influences the nucleation process of $A\beta_{1-40}$ while aggregate morphology or mass were presumably determined by $A\beta_{1-40}$ (Fig. 5C). Titration of $A\beta_{1-38}$ with $A\beta_{1-42}$ similarly lead to a decreased nucleation rate but, in addition, gradually increased the elongation rate and final ThT fluorescence intensity (Fig. 5B,D). The complex aggregation characteristics compared to each of these peptides in isolation are highly suggestive of interaction of the Aβ peptides in mixtures.

$A\beta_{1-40}$ is the most predominant species recovered from cerebrospinal fluid (CSF) (6,45). $A\beta_{1-38}$ has been reported to be present in CSF at concentrations of 1.26 to 2.78 ng/ml, while concentrations of $A\beta_{1-42}$ were 0.46 to 2.07 ng/ml (6,45,46). Quantitative detection of $A\beta_{1-43}$ has only been performed in brain plaques and, as suitable antibodies are not available, can generally not be distinguished from that of $A\beta_{1-42}$. While quantitative information on the released amounts of the four Aβ isoforms of interest from APP is only available for FAD mutations based on *in vitro* observations (11,44,47,48), we performed titration assays (Fig. 5). Results indicated that 30 % of $A\beta_{1-38}$ or $A\beta_{1-43}$ already caused significant alteration of the aggregation profile of $A\beta_{1-42}$ and of the lag phase of $A\beta_{1-40}$. Many FAD-related mutations accumulate $A\beta_{1-42}$ while it can be assumed that in sporadic AD $A\beta_{1-40}$ is predominantly produced (49). We therefore decided to evaluate the effect of small concentrations (10 %) of $A\beta_{1-38}$ and $A\beta_{1-43}$ on predominantly present (90 %) $A\beta_{1-40}$ and $A\beta_{1-42}$ to monitor more subtle influences of the presence of peptides in mixtures. In summary, we evaluated oligomerization, cytotoxicity and aggregation of 9:1 mixtures of $A\beta_{1-40}$:$A\beta_{1-38}$, $A\beta_{1-40}$:$A\beta_{1-43}$, $A\beta_{1-42}$:$A\beta_{1-38}$, and $A\beta_{1-42}$:$A\beta_{1-43}$. At these low concentrations the effect of the addition of $A\beta_{1-38}$ and $A\beta_{1-43}$ to either $A\beta_{1-40}$ or $A\beta_{1-42}$ was limited to a significant decrease in final fluorescence intensity while leaving the nucleation phase unchanged (Fig. 6A,B). Visualization of aggregate morphology by TEM further rationalized the observed change in final fluorescence intensity (Fig. 1C,6C). Even though aggregate formation could not be established at early time points for $A\beta_{1-38}$ and $A\beta_{1-40}$ in isolation, a 9:1 mixture of these peptides showed the formation of extensive ThT-negative but A11-positive aggregates that were present for extended periods of time (Fig.

6A,C,D). Also at early time points of incubation the morphologies of both $A\beta_{1-40}$ and $A\beta_{1-42}$ in mixtures (Fig. 6C) appear different from these peptides in isolation (compare with Fig. 1C). Upon extended incubation all mixtures aggregated into morphologically similar networks of long, interacting fibrils, similar to those observed for peptides in isolation (Fig. 6C). The observed differences in A11-interaction and aggregate morphology further led us to investigate the cytotoxic response of Aβ mixtures using cultured SH-SY5Y cells. Interestingly, even though $A\beta_{1-38}$ or $A\beta_{1-40}$ in isolation induced no cytotoxic response below a concentration of 20 μM, the addition of $A\beta_{1-38}$ to $A\beta_{1-40}$ resulted in a pronounced and significant loss of cell viability at a total peptide concentration of 10 μM, consistent with the A11-positive response for this mixture (Fig. 6D,E). Strikingly, the addition of $A\beta_{1-38}$ to $A\beta_{1-42}$ instead exerted a cytoprotective effect, despite showing the formation of A11-positive oligomers, preventing loss of cell viability up to a total Aβ concentration of 10 μM. In addition to this, even though both $A\beta_{1-42}$ and $A\beta_{1-43}$ are similarly cytotoxic at a concentration of 10 μM, the mixture of these two peptides alleviates the cytotoxic response while $A\beta_{1-43}$ induces cytotoxicity in the presence of $A\beta_{1-40}$.

Collectively, our data suggest that, apart from distinct propensities to form cytotoxic oligomers and aggregates for individual Aβ peptides, mixtures of various Aβ peptides do not behave in a predictable manner according to a simple additive effect but can actively modulate the behavior of other isoforms present in the mixture to either induce or prevent toxicity or modify their aggregation propensities.

DISCUSSION

Aβ aggregation is a complex process during which a monomeric population progressively self-assembles first into oligomers and finally into mature fibrils. We show that biologically relevant mixtures of Aβ peptides, containing $A\beta_{1-38}$, $A\beta_{1-40}$, $A\beta_{1-42}$, and $A\beta_{1-43}$, behave in a more complex manner than can be anticipated from their behaviors in isolation with direct consequences for their oligomerization, aggregation and cytotoxic behavior. We also report that co-occurring Aβ peptides can affect each other by conformational modulation of the C-terminal region which, in

turn, is a function of C-terminal flexibility to adopt various conformations. For example, $A\beta_{1-38}$ in isolation exhibited little cytotoxic potential, similar to $A\beta_{1-40}$. At the same time, cytotoxic oligomers accumulated rapidly for $A\beta_{1-42}$, and $A\beta_{1-43}$. Nevertheless, mixtures of $A\beta_{1-38}$ and $A\beta_{1-40}$ were highly toxic while the addition of $A\beta_{1-38}$ to $A\beta_{1-42}$ surprisingly induced a cytoprotective effect. The A11 reactivity of the individual $A\beta$ peptides in isolation correlated with the observed cytotoxicity although all isoforms were found to form oligomers. This observation suggests a conformational difference between oligomers of different isoforms. The presence of both toxic, A11-positive and non-toxic, A11-negative oligomers has been reported recently for $A\beta$ as well as for the yeast-sup35 protein (50,51). The cytotoxicity - A11 reactivity correlation for peptides in isolation could not be extended to mixtures of $A\beta$ isoforms. This lack of correlation can be explained by the polyclonal nature of the antibody to recognize non-toxic oligomers in addition to toxic species. Another possibility is that non-toxic and toxic oligomers are both formed and that the variation in signal intensities, and cytotoxicity, arises from the variation in the distribution between these oligomers. At high concentrations when the level of toxic oligomers is sufficiently high, the shorter $A\beta$ isoforms become similar cytotoxic to the longer $A\beta$ isoforms. While not being able to reveal distinct accumulation of specific conformations using CD, FT-IR revealed small structural differences during a 1.5 h incubation time. Even though all tested $A\beta$ peptides showed substantial β-sheet formation over time, only for $A\beta_{1-38}$ and $A\beta_{1-43}$ anti-parallel β-sheet formation could be identified which has been interpreted previously as typical for oligomer formation (42). As both FT-IR and CD are only informative on an ensemble level, we used MD to elucidate the short-time scale dynamic behavior of the peptides. MD simulations revealed that both $A\beta_{1-38}$ and $A\beta_{1-42}$ gained extended β-sheet conformation rapidly while helicity in $A\beta_{1-40}$ was retained for longer which is in good agreement with earlier reports (52). In line with our findings, it has previously been reported that stabilization of the central α-helical region of $A\beta$ by ligands or mutations results in significant delay of aggregation (53-55), and that inhibition of unfolding of the central α-helical region increases

longevity in a *Drosophila* model of AD (54). At the same time, rapid induction of extended β-sheet formation has been found to have strong predictive power in terms of toxic potential rationalizing the development of so-called β-sheet breakers as therapeutic approach (reviewed in 56). Interestingly, $A\beta_{1-38}$ showed behavior that could be explained by rapid gain and loss of extended β-sheet conformation, fluctuating in behavior between $A\beta_{1-40}$ and $A\beta_{1-42}$/$A\beta_{1-43}$, respectively. Rapid conformational switching between distinct conformations has been observed before for synaptically confined proteins SNAP-25 and synaptobrevin and was proposed to characterize a specific class of intrinsically disordered proteins (57). Conformational flexibility was suggested to allow for fast ligand interaction and conformational selection which potentially has functional implications for the findings we report on $A\beta_{1-38}$ but which warrant further investigation. The presence of other peptides with higher preference of one over another conformation may drive $A\beta_{1-38}$ to rapidly recognize these as a potential ligand and template for conformational selection, which, in turn, either induces or inhibits aggregation. However, this may be an oversimplification of the actual situation since $A\beta_{1-42}$ in the presence of $A\beta_{1-38}$ is in fact less toxic which does not comply with this suggestion. Further research is required to precisely underpin the molecular mechanism of this observation. It has been previously reported that Glu^{22}, Asp^{23} and Lys^{28} play a critical role in the aggregation process (58-61). Presumably, Asp^{23} (and Lys^{28}), while residing in a helical conformation, may not be able to trigger the formation of extended conformations, at least at early time points, thus retarding the aggregation of $A\beta_{1-40}$. Therefore, not only the unfolding rate of the C-terminus, as has been previously suggested, can dictate the potential event to trigger aggregation and toxicity of $A\beta$ (60), but also the capability of a given $A\beta$ peptide to retain its helical conformation may be considered to induce such events. Based on the outcome of our MD simulations we suggest that the plastic behavior of $A\beta_{1-38}$, inducing toxicity for $A\beta_{1-40}$ while eliminating response to $A\beta_{1-42}$, plays a key role to these observations. Hence, the presence of other peptides may direct the self-assembly process toward at least two possible pathways, one leading to toxic oligomers and the second leading

to non-toxic intermediates. $A\beta_{1-43}$ does not display fluctuating secondary structures, and rapidly forms extended β-sheets. The self-assembly process in presence of other peptides is therefore probably more dependent on the flexibility of the structure of the second peptide. Indeed, it has been shown for the N-terminal domain of the HypF protein from *Escherichia coli* that both toxic and non-toxic oligomers can be formed (62).

Overall, our results can be of major importance for the further development of therapeutic strategies. The current approach of modulating γ-secretase activity to decrease $A\beta_{1-42}$ generation results in increased $A\beta_{1-38}$ levels at the same time. This approach is based on the observation that longer Aβ isoforms are more aggregation-prone. Hence, establishing an increased $A\beta_{1-38}$ level is considered a suitable and non-toxic approach to inhibit AD disease progress without compromising the important multi-substrate processing by γ-

secretase. However, clinical studies still have to confirm their disease-modulating capacity. Whether this is due to the low brain-barrier penetrating potency of the compounds being tested requires further investigation. Together with previously published data (44), our results possibly indicate that another explanation for the lack of clinical evidence to place GSMs firmly on the map as Alzheimer disease therapy may be the induction of adverse, unexpected events as a result of the increased $A\beta_{1-38}$ levels in combination with other Aβ peptides. In this view, Golde and colleagues (63) recently argued that the efficiency of different GSMs to shift Aβ release towards shorter isoforms could determine their therapeutic potential. We propose that peptide conformational flexibility may confer toxic properties to its oligomers and underline the importance of understanding the interplay between various Aβ isoforms.

REFERENCES

1. Glenner, G. and Wong, C. (1984) Alzheimer's disease: initial report of the purification and characterization of a novel cerebrovascular amyloid protein. *Biochem. Biophys. Res. Commun.* **120**, 885-890

2. Haass, C., Schlossmacher, M. G., Hung, A. Y., Vigo-Pelfrey, C., Mellon, A., Ostaszewski, B. L., Lieberburg, I., Koo, E. H., Schenk, D., and Teplow, D. B. (1992) Amyloid β-peptide is produced by cultured cells during normal metabolism. *Nature* **359**, 322-325

3. De Strooper, B., Saftig, P., Craessaerts, K., Vanderstichele, H., Guhde, G., Annaert, W., von Figura, K., and van Leuven, F. (1998) Deficiency of presenilin-1 inhibits the normal cleavage of amyloid precursor protein. *Nature* **391**, 387-390

4. Yan, R., Bienkowski, M. J., Shuck, M. E., Miao, H., Tory, M. C., Pauley, A. M., Brashier, J. R., Stratman, N. C., Mathews, W. R., Buhl, A. E., Carter, D. B., Tomasselli, A. G., Parodi, L. A., Heinrikson, R. L., and Gurney, M. E. (1999) Membrane-anchored aspartyl protease with Alzheimer's disease β-secretase activity. *Nature* **402**, 533-537

5. Vigo-Pelfrey, C., Lee, D., Keim, P., Lieberburg, I., and Schenk, D. B. (1993) Characterization of β-amyloid peptide from human cerebrospinal fluid. *J. Neurochem.* **61**, 1965-1968

6. Wiltfang, J., Esselmann, H., Bibl, M., Smirnov, A., Otto, M., Paul, S., Schmidt, B., Klafki, H. W., Maler, M., Dyrks, T., Bienert, M., Beyermann, M., Rüther, E., and Kornhuber, J. (2002) Highly conserved and disease-specific patterns of carboxyterminally truncated Aβ peptides 1-37/38/39 in addition to 1-40/42 in Alzheimer's disease and in patients with chronic neuroinflammation. *J. Neurochem.* **81**, 481-496

7. Gu, Y., Misonou, H., Sato, T., Dohmae, N., Takio, K., and Ihara, Y. (2001) Distinct intramembrane cleavage of the β-amyloid precursor protein family resembling γ-secretase-like cleavage of Notch. *J. Biol. Chem.* **276**, 35235-35238

8. Sato, T., Dohmae, N., Kakuda, N., Misonou, H., Mitumori, R., Maruyama, H., Koo, E. H., Haass, C., Takio, K., Morishima-Kawashima, M., Ishiura, S., and Ihara, Y. (2003) Potential link between amyloid β-protein 42 and C-terminal fragment γ 49-99 of β-Amyloid Precursor Protein. *J. Biol. Chem.* **278**, 24294-24301

9. Qi-Takahara, Y., Morishima-Kawashima, M., Tanimura, Y., Dolios, G., Hirotani, N., Horikoshi, Y., Kametani, F., Maeda, M., Saido, T. C., Wang, R., and Ihara, Y. (2005) Longer forms of amyloid β protein: implications for the mechanism of intramembrane cleavage by γ-secretase. *J. Neurosci.* **25**, 436-445

10. Takami, M., Nagashima, Y., Sano, Y., Ishihara, S., Morishima-Kawashima, M., Funamoto, S., and Ihara, Y. (2009) γ-secretase: successive tripeptide and tetrapeptide release from the transmembrane domain of β-carboxyl terminal fragment. *J. Neurosci.* **29**, 13042-13052

11. Bentahir, M., Nyabi, O., Verhamma, J., Tolia, A., Horne, K., Wiltfang, J., Esselmann, H., and De Strooper, B. (2006) Presenilin clinical mutations can affect γ-secretase activity by different mechanisms. *J. Neurochem.* **96**, 732-742

12. Saito, T., Suemoto, T., Brouwers, N., Sleegers, K., Funamoto, S., Mihira, N., Matsuba, Y., Yamada, K., Nilsson, P., Takano, J., Nishimura, M., Iwata, N., Van Broeckhoven, C., Ihara, Y., and Saido, T. C. (2011) Potent amyloidogenicity and pathogenicity of Aβ43. *Nat. Neurosci.* **14**, 1023-1032

13. Jarrett, J. T. and Lansbury, P. T. (1993) Seeding "one-dimensional crystallization" of amyloid: a pathogenic mechanism in Alzheimer's disease and scrapie? *Cell* **73**, 1055-1058

14. Bitan, G., Kirkitadze, M. D., Lomakin, A., Vollers, S. S., Benedek, G. B., and Teplow, D. B. (2003) Amyloid β-protein (Aβ) assembly: Aβ40 and Aβ42 oligomerize through distinct pathways. *Proc. Natl. Acad. Sci. USA* **100**, 330-335

15. Benseny-Cases, N., Cocera, M., and Cladera, J. (2007) Conversion of non-fibrillar β-sheet oligomers into amyloid fibrils in Alzheimer's disease amyloid peptide aggregation. *Biochem. Biophys. Res. Commun.* **361**, 916-921

16. Gravina, S., Ho, L., Eckman, C. B., Long, K. E., Otvos, L., Younkin, L. H., Suzuki, N., and Younkin, S. G. (1995) Amyloid β protein (Aβ) in Alzheimer's disease brain. Biochemical and immunocytochemical analysis with antibodies specific for forms ending at Aβ 40 or Aβ42(43). *J. Biol. Chem.* **270**, 7013-7016

17. Iwatsubo, T., Saido, T. C., Mann, D. M., Lee, V. M., and Trojanowski, J. Q. (1996) Full-length amyloid-β(1-42 (43)) and amino-terminally modified and truncated amyloid-β42 (43) deposit in diffuse plaques. *Am. J. Pathol.* **149**, 1823-1830

18. Welander, H., Franberg, J., Graff, C., Sundström, E., Winblad, B., and Tjernberg, L. O. (2009) Aβ43 is more frequent than Aβ40 in amyloid plaque cores from Alzheimer disease brains. *J. Neurochem.* **110**, 697-706

19. Weggen, S., Eriksen, J. L., Das, P., Sagi, S. A., Wang, R., Pietrzik, C. U., Findlay, K. A., Smith, T. E., Murphy, M. P., Bulter, T., Kang, D. E., Marquez-Sterling, N., Golde, T. E., and Koo, E. H. (2001) A subset of NSAIDs lower amyloidogenic Aβ42 independently of cyclooxygenase activity. *Nature* **414**, 212-216

20. Eriksen, J. L., Sagi, S. A., Smith, T. E., Weggen, S., Das, P., McLendon, D. C., Ozols, V. V., Jessing, K. W., Zavitz, K. H., Koo, E. H., and Golde, T. E. (2003) NSAIDs and enantiomers of flurbiprofen target γ-secretase and lower Aβ42 in vivo. *J. Clin. Invest.* **112**, 440-449

21. Laino, C. (2009) In follow-up analysis of clinical trial, NSAIDs seem to preserve cognitive function in patients with healthy brains. *Neurol. Today* **9**, 21-22

22. Oehlrich, D., Berthelot, D., and Gijsen, H. (2011) γ-Secretase modulators as potential disease modifying anti-Alzheimer's drugs. *J. Med. Chem.* **54**, 669-698

23. Imbimbo, B. P. and Giardina, G. A. M. (2011) γ-Secretase inhibitors and modulators for the treatment of Alzheimer's disease: disappointments and hopes. *Curr. Top. Med. Chem.* **11**, 1555-1570

24. Lewczuk, P., Esselmann, H., Meyer, M., Wollscheid, V., Neumann, M., Otto, M., Maler, J. M., Rüther, E., Kornhuber, J., and Wiltfang, J. (2003) The amyloid-β (Aβ) peptide pattern in cerebrospinal fluid in Alzheimer's disease: evidence of a novel carboxyterminally elongated Aβ peptide. *Rapid Commun. Mass Spectrom.* **17**, 1291-1296

25. Maddalena, A. S., Papassotiropoulos, A., Gonzalez-Agosti, C., Signorell, A., Hegi, T., Pasch, T., Nitsch, R. M., and Hock, C. (2004) Cerebrospinal fluid profile of amyloid β peptides in patients with Alzheimer's disease determined by protein biochip technology. *Neurodegenerative Dis.* **1**, 231-235

26. Kuperstein, I., Broersen, K., Benilova, I., Rozenski, J., Jonckheere, W., Debulpaep, M., Vandersteen, A., Segers-Nolten, I., van der Werf, K., Subramaniam, V., Braeken, D., Callewaert, G., Bartic, C., D'Hooge, R., Martins, I. C., Rousseau, F., Schymkowitz, J., and De Strooper, B. (2010) Neurotoxicity of Alzheimer's disease Aβ peptides is induced by small changes in the $Aβ_{42}$ to $Aβ_{40}$ ratio. *EMBO J.* **29**, 3408-3420

27. Broersen, K., Jonckheere, W., Rozenski, J., Vandersteen, A., Pauwels, K., Pastore, A., Rousseau, F., and Schymkowitz, J. (2011) A standardized and biocompatible preparation of aggregate-free amyloid β peptide for biophysical and biological studies of Alzheimer's disease. *Protein Eng. Des. Sel*. **24**, 743-750

28. Kayed, R., Head, E., Thompson, J. L., McIntire, T. M., Milton, S. C., Cotman, C. W., and Glabe, C. G. (2003) Common structure of soluble amyloid oligomers implies common mechanism of pathogenesis. *Science* **300**, 486-489

29. Fernandez-Escamilla, A. M., Rousseau, F., Schymkowitz, J., and Serrano, L. (2004) Prediction of sequence-dependent and mutational effects on the aggregation of peptides and proteins. *Nat. Biotechnol.* **22**, 1302-1306

30. Kang, J., Lemaire, H. G., Unterbeck, A., Salbaum, J. M., Masters, C. L., Grzeschik, K. H., Multhaup, G., Beyreuther, K., and Müller-Hill, B. (1987) The precursor of Alzheimer's disease amyloid A4 protein resembles a cell-surface receptor. *Nature* **325**, 733-736

31. Jorgensen, W. L. and Tirado-Rives, J. (1988) The OPLS potential functions for proteins, energy minimizations for crystals of cyclic peptides and crambin. *J. Am. Chem. Soc.* **110**, 1657-1666

32. Hess, B., Bekker, H., Berendsen, H. J. C., and Fraaije, J. G. E. M. (1997) LINCS: A linear constraint solver for molecular simulations. *J. Comput. Chem.* **18**, 1463-1472

33. Pettersen, E. F., Goddard, T. D., Huang, C. C., Couch, G. S., Greenblatt, D. M., Meng, E. C., and Ferrin, T. E. (2004) UCSF Chimera--a visualization system for exploratory research and analysis. *J. Comput. Chem.* **25**, 1605-1612

34. Harper, J. D. and Lansbury, P.T. (1997) Models of amyloid seeding in Alzheimer's disease and scrapie: mechanistic truths and physiological consequences of the time-dependent solubility of amyloid proteins. *Annu. Rev. Biochem.* **66**, 385-407

35. Biancalana, M. and Koide, S. (2010) Molecular mechanism of Thioflavin-T binding to amyloid fibrils. *Biochim. Biophys. Acta* **1804**, 1405-1412

36. Stine, W. B., Dahlgren, K. N., Krafft, G. A., LaDu, M. J. (1996) The nanometer-scale structure of amyloid-β visualized by atomic force microscopy. *J. Prot. Chem.* **15**, 193-203

37. Röhrig, U. F., Laio, A., Tantalo, N., Parrinello, M., and Petronzio, R. (2006) Stability and structure of oligomers of the Alzheimer β peptide Aβ$_{16-22}$: from the dimer to the 32-mer. *Biophys. J.* **91**, 3217-3229

38. Levine, H. III (1993) Thioflavine T interaction with synthetic Alzheimer's disease β-amyloid peptides: Detection of amyloid aggregation in solution. *Prot. Sci.* **2**, 404-410

39. Lambert, M. P., Barlow, A. K., Chromy, B. A., Edwards, C., Freed, R., Liosatos, M., Morgan, T. E., Rozovsky, I., Trommer, B., Viola, K. L., Wals, P., Zhang, C., Finch, C. E., Krafft, G. A., and Klein, W. L. (1998) Diffusible, nonfibrillar ligands derived from Aβ$_{1-42}$ are potent central nervous system neurotoxins. *Proc. Natl. Acad. Sci. USA* **95**, 6448-6453

40. Lesné, S., Koh, M. T., Kotilinek, L., Kayed, R., Glabe, C. G., Yang, A., Gallagher, M., and Ashe, K. H. (2006) A specific amyloid-β protein assembly in the brain impairs memory. *Nature* **440**, 352-357

41. Ahmed, M., Davis, J., Aucoin, D., Sato, T., Ahuja, S., Aimoto, S., Elliott, J. I., Van Nostrand, W. E., and Smith, S. O. (2010) Structural conversion of neurotoxic amyloid-β$_{1-42}$ oligomers to fibrils. *Nat. Struct. Mol. Biol.* **17**, 561-567

42. Cerf, E., Sarroukh, R., Tamamizu, S., Breydo, L., Derclaye, S., Dufrêne, Y. F., Narayanaswami, V., Goormaghtigh, E., Ruysschaert, J.M., and Raussens, V. (2009). Antiparallel β-sheet: a signature structure of the oligomeric amyloid β-peptide. *Biochem. J.* **421**, 415-423

43. Kabsch, W. and Sander, C. (1983) Dictionary of protein secondary structure: pattern recognition of hydrogen-bonded and geometrical features. *Biopolymers* **22**, 2577-2637

44. Chávez-Gutiérrez, L., Bammens, L., Benilova, I., Vandersteen, A., Benurwar, M., Borgers, M., Lismont, S., Zhou, L., Van Cleynenbreugel, S., Esselmann, H., Wiltfang, J., Serneels, L., Karran, E., Gijsen, H., Schymkowitz, J., Rousseau, F., Broersen, K., and De Strooper, B. (2012) The mechanism of γ-secretase dysfunction in familial Alzheimer disease. *EMBO J.* **31**, 2261-2274

45. Bibl, M., Mollenhauer, B., Wolf, S., Esselmann, H., Lewczuk, P., Kornhuber, J., and Wiltfang, J. (2007) Reduced CSF carboxyterminally truncated Aβ peptides in frontotemporal lobe degenerations. *J. Neural. Transm.* **114**, 621-628

46. Mann, D. M. A., Iwatsubo, T., Ihara, Y., Cairns, N. J., Lantos, P. L., Bogdanovic, N., Lannfelt, L., Winblad, B., Maat-Schieman, M. L. C., and Rossor, M. N. (1996) Predominant deposition of amyloid-β42(43) in plaques in cases of Alzheimer's disease and hereditary cerebral hemorrhage associated with mutations in the amyloid precursor protein gene. *Am. J. Pathol.* **148**, 1257-1266

47. Scheuner, D. Eckman, C., Jensen, M., Song, X., Citron, M., Suzuki, N., Bird, T.D., Hardy, J., Hutton, M., Kukull, W., Larson, E. Levy-Lahad, E., Viitanen, M., Peskind, E., Poorkay, P., Schellenberg, G., Tanzi, R., Wasco, W., Lannfelt, L., Selkoe, D., and Younkin, S. (1996) Secreted amyloid beta-protein similar to that in the senile plaques of Alzheimer's disease is increased in vivo by the presenilin 1 and 2 and APP mutations linked to familial Alzheimer's disease. *Nature Med.* **2**, 864-870

48. Citron, M., Westaway, D., Xia, W., Carlson, G., Diehl, T., Levesque, G., Johnson-Wood, K., Lee, M., Seubert, P., Davis, A., Kholodenko, D., Motter, R., Sherrington, R., Perry, B., Yao, H., Strome, R., Lieberburg, I., Rommens, J., Kim, S., Schenk, D., Fraser, P., St Georgy Hyslop, P., and Selkoe,

D.J. (1997) Mutant presenilins of Alzheimer's disease increase production of 42-residue amyloid β-protein in both transfected and transgenic mice. *Nature Med.* **3**, 67-72.

49. Younkin, S. G. (1998) The role of Abeta42 in Alzheimer's disease. *J. Physiol. Paris* **92**, 289-292

50. Krishnan, R., Goodman, J. L., Mukhopadhyay, S., Pacheco, C. D., Lemke, E. A., Deniz, A. A., and Lindquist, S. (2012) Conserved features of intermediates in amyloid assembly determine their benign or toxic states. *Proc. Natl. Acad. Sci. USA* **109**, 11172-11177

51. Ladiwala, A. R. A., Litt, J., Kane, R. S., Aucoin, D. S., Smith, S. O., Ranjan, S., Davis, J., Van Nostrand, W. E., and Tessier, O. M. (2012) Conformational differences between two amyloid β oligomers of similar size and dissimilar toxicity. *J. Biol. Chem.* **287**, 24765-24773

52. Shen, L., Ji, H. -F., and Zhang, H. -Y. (2008) Why is the C-terminus of Aβ(1-42) more unfolded than that of Aβ(1-40)? Clues from hydrophobic interaction. *J. Phys. Chem. B.* **112**, 3164-3167

53. Päiviö, A., Nordling, E., Kallberg, Y., Thyberg, J., and Johansson, J. (2004) Stabilization of discordant helices in amyloid fibril-forming proteins. *Prot. Sci.* **13**, 1251-1259

54. Nerelius, C., Sandegren, A., Sargsyan, H., Raunak, R., Leijonmarck, H., Chatterjee, U., Fisahn, A., Imarisio, S., Lomas, D. A., Crowther, D. C., Strömberg, R., and Johansson, J. (2009) α-Helix targeting reduces amyloid-β peptide toxicity. *Proc. Natl. Acad. Sci. USA* **106**, 9191-9196

55. Ito, M., Johansson, J., Strömberg, R., and Nilsson, L. (2011) Unfolding of the amyloid β-peptide central helix: mechanistic insights from molecular dynamics simulations. *PLoS ONE* **6**, e17587

56. Wisniewski, T. and Sadowski, M. (2008) Preventing β-amyloid fibrillization and deposition: β-sheet breakers and pathological chaperone inhibitors. *BMC Neurosci.* **3**:9 Suppl 2:S5

57. Choi, U. B., McCann, J. J., Weninger, K. R., and Bowen, M. E. (2011) Beyond the random coil: stochastic conformational switching in intrinsically disordered proteins. *Structure* **19**, 566-576

58. Borreguero, J. M., Urbanc, B., Lazo, N. D., Buldyrev, S. V., Teplow, D. B., and Stanley, H. E. (2005) Folding events in the 21-30 region of amyloid β-protein (Aβ) studied in silico. *Proc. Natl. Acad. Sci. USA* **102**, 6015-6020

59. Lazo, N., Grant, M., Condron, M., Rigby, A., and Teplow, D. (2005) On the nucleation of amyloid β-protein monomer folding. *Protein Sci.* **14**, 1581-1596

60. Baumketner, A., Bernstein, S. L., Wyttenbach, T., Lazo, N. D., Teplow, D. B., Bowers, M. T., and Shea J.-E. (2006) Structure of the 21-30 fragment of amyloid β-protein. *Prot. Sci.* **15**, 1239-1247

61. Masman, M. F., Eisel, U. L. M., Csizmadia, I. G., Penke, B., Enriz, R. D., Marrink, S. J., and Luiten, P. G. M. (2009) In silico study of full-length amyloid β 1-42 tri- and penta-oligomers in solution. *J. Phys. Chem. B.* **113**, 11710-11719

62. Campioni, S., Mannini, B., Zampagni, M., Pensalfini, A., Parrini, C., Evangelisti, E., Relini, A., Stefani, M., Dobson, C. M., Cecchi, C., and Chiti, F. (2010) A causative link between the structure of aberrant protein oligomers and their toxicity. *Nat. Chem. Biol.* **6**, 140-147

63. Golde, T., Ran, Y., and Felsenstein, K. (2012) Shifting a complex debate on γ-secretase cleavage and Alzheimer's disease. *EMBO J.* **31**, 2237-2239

FOOTNOTES

The abbreviations used are: AD, Alzheimer's disease; APP, amyloid precursor protein; PS1, presenilin 1; GSI, γ-secretase inhibitor; GSM, γ-secretase modulator; ThT, thioflavin T; TEM, transmission electron microscopy; AFM, atomic force microscopy; CD, circular dichroism; MD, molecular dynamics; DSSP, definition of secondary structure of proteins; CSF, cerebrospinal fluid; ESI-MS, electrospray ionization mass spectrometry; HFIP, 1,1,1,3,3,3-hexafluor-2-propanol; DMSO, dimethyl sulfoxide.

FIGURE LEGENDS

FIGURE 1. Carboxy-terminal heterogeneity affects aggregation kinetics of the Aβ peptide. (A) ThT fluorescence was recorded *in situ* every 5 min at 25 °C. $A\beta_{1-38}$ (continuous black line) and $A\beta_{1-40}$ (continuous grey line) display a lag phase while $A\beta_{1-42}$ (dotted black line) and $A\beta_{1-43}$ (dotted grey line) induce ThT fluorescence almost immediately. The values represent the means of three experiments. (B) Final (10 h) ThT fluorescence intensities derived from panel A. Statistical significance (unpaired 2-tailed t-test) compared to the $A\beta_{1-38}$ value is indicated by *** $P<0.0001$, ** $P<0.0005$ or * $P<0.005$. (C) After 0.5 h incubation $A\beta_{1-42}$ and $A\beta_{1-43}$ formed networks while $A\beta_{1-38}$ and $A\beta_{1-40}$ do not show visible aggregates. After 4 h incubation $A\beta_{1-38}$ and $A\beta_{1-40}$ formed 8-12 nm wide, extended, negatively stained fibrils. $A\beta_{1-42}$ organized into a network of rigid 14-16 nm wide fibrils. For $A\beta_{1-43}$ a mixture of protofibrils and fibrils were observed. After 24 h all Aβ formed similar fibrillar networks. Scalebar: 200 nm. (D) Total TANGO scores indicated an increasing overall aggregation propensity of Aβ with increasing peptide length. 37 to 40 amino acids long peptides deviated from this trend. Peptides studied in this manuscript are marked. (E) Sequence based prediction of aggregation prone stretches by the TANGO algorithm suggests a common aggregating region in the core of the peptide and a second aggregating region at the C-terminus. Differences in total TANGO score (Fig. 1D) are exclusively due to the C-terminal aggregating region. $A\beta_{1-38}$ (continuous black line) and $A\beta_{1-40}$ (continuous grey line) display similar predicted aggregation propensity while that of $A\beta_{1-42}$ (dotted black line) and $A\beta_{1-43}$ (dotted grey line) were higher.

FIGURE 2. Differences in aggregation kinetics due to C-terminal heterogeneity are reflected at toxic oligomer level. Aβ at 50 μM was allowed to aggregate at 25 °C under quiescent conditions. (A) Analysis with the A11 oligomer-specific antibody detected oligomeric $A\beta_{1-42}$ and $A\beta_{1-43}$ after as little as 0.5 h incubation whereas $A\beta_{1-38}$ and $A\beta_{1-40}$ became A11-positive after 5 to 6 h of incubation. (B) Imaging using AFM indicated the presence of oligomers for all Aβ samples incubated for 1.5 h. The length of the bar represents 500 nm. (C) Pre-incubated (1.5 h) Aβ was added to cultured SH-SY5Y cells and incubated for 24 h before probing cytotoxicity using Cell Titer Blue viability assay. $A\beta_{1-38}$ (black) and $A\beta_{1-40}$ (dark grey) only cause cytotoxicity at a concentration of 20 μM while $A\beta_{1-42}$ (light grey) and $A\beta_{1-43}$ (white) are significantly cytotoxic at a concentration of 5 μM. Values are expressed as percent of cell viability ± SD (N=4), buffer signal was normalized to 100 %. Statistical significance (unpaired 2-tailed t-test) compared to buffer control values (normalized to 100 %) is indicated by p-value analysis similar to Fig. 1B.

FIGURE 3. Aggregating Aβ peptides show differences on a secondary structural level. (A) CD measurements were performed with pre-incubated (1.5 h) Aβ at 15 μM. Spectra recorded for Aβ$_{1-38}$ (continuous black line) and Aβ$_{1-40}$ (continuous grey line) were characteristic of peptides with a large degree of disorder whereas Aβ$_{1-42}$ (dotted black line) and Aβ$_{1-43}$ (dotted grey line) displayed curves with a single minimum at 217 nm, suggesting β-sheet formation. High buffer interference was observed at wavelengths < 207 nm (B) FT-IR absorbance was measured of monomeric and pre-incubated (1.5 h) Aβ at 200 μM and the difference between both spectra was plotted. The difference spectra showed an intensity increase at a wavelength of 1627 cm^{-1} indicating that all four peptides were converted into a β-sheet conformation. For Aβ$_{1-38}$ (continuous black line), and Aβ$_{1-43}$ (dotted grey line) an additional increase in intensity around 1695 cm^{-1} was observed implying an antiparallel oriented β-sheet. Aβ$_{1-40}$ (continuous grey line) and Aβ$_{1-42}$ (dotted black line) data were both characterized by a loss of β-turn as observed by the decrease in intensity at 1680 cm^{-1}.

FIGURE 4. Aβ peptides show conformational fluctuations at short time-scales, which vary upon C-terminal elongation. Secondary structure composition determined by DSSP method: extended conformation (β-bridge plus β-sheet structures), and helical conformation (α-helix plus 3$_{10}$-helix plus π-helix). Results were averaged over ten independent simulations. The extended conformation content in function of time for Aβ$_{1-38}$ (continuous black line) is compared to: (A) Aβ$_{1-40}$ (continuous grey line); and (B) Aβ$_{1-42}$ (dotted black line); inset plot (B1) Aβ$_{1-43}$ (dotted grey line), which reveals a similar profile compared to Aβ$_{1-42}$. Statistically significant differences (SEM) are denoted with a caped-line (## P<0.005). (C) The helical content in function of time is shown for all peptides. Color code is the same as for the previous panels. Regions of the simulation time wherein there are statistically significant differences are denoted with a caped-line (## P<0.005) compared to Aβ$_{1-42}$. Inset plot (C1) shows helicity per residue for all Aβ peptides (## P<0.005, compared to all Aβ peptides). Helicity is reported as the percentage of simulation time that a given amino acid residue presented α-helix conformation. (D) Snapshots for all Aβ peptides at 0, 25, 50, 75 and 100 ns of simulation time. C-termini positions are denoted with an asterisk (*).

FIGURE 5. Little prevalent Aβ peptides strongly affect the behavior of predominant Aβ. ThT fluorescence was recorded *in situ* every 5 min at 25 °C with 50 μM Aβ and 12 μM ThT. Values represent means of two experiments. (A, C) Irrespective of its concentration, Aβ$_{1-43}$ (dotted grey line) reduced the lag-phase for aggregation (C1) of Aβ$_{1-40}$ (continuous grey line) without affecting elongation rates (C2). Aβ$_{1-40}$:Aβ$_{1-43}$ mixtures displayed higher fluorescence intensity after 8 h incubation (C3) than Aβ$_{1-40}$ and Aβ$_{1-43}$ alone. Color code as in Fig. 5A. (B, D) Titration of Aβ$_{1-42}$ (dotted black line) with Aβ$_{1-38}$ (continuous black line) reduced lag phase (D1), and elongation rate (D2) but increased fluorescence intensity at plateau (D3). Color code as in Fig. 5B.

FIGURE 6. Aβ peptides in mixtures display complex aggregation behavior and toxicity. (A, B) Addition of 10 % (= 5 μM) Aβ$_{1-38}$ (continuous black line) or Aβ$_{1-43}$ (dotted grey line) to 90 % (= 45 μM) Aβ$_{1-40}$ (continuous grey line) or Aβ$_{1-42}$ (dotted black line) decreased final (10 h) ThT fluorescence compared to Aβ$_{1-40}$ or Aβ$_{1-42}$ alone. Values represent means of three experiments (C) After 1.5 h of incubation mixtures containing Aβ$_{1-38}$ formed amorphous aggregates while mixtures containing Aβ$_{1-43}$ formed short fibrillar structures. Longer incubation for 6 h resulted in fibrillar networks for all mixtures which extended into dense, highly intertwined, stained networks after 24 h of incubation. Length of scale bar is 200 nm. (D) All Aβ mixtures intensively reacted with A11 oligomer-specific antibody after 0.5 h of incubation which gradually decreased upon longer incubation dependent on the Aβ mixture (E) Aβ was added to cultured SH-SY5Y cells and incubated for 24 h before probing cytotoxicity using the Cell Titer Blue viability assay. Note that non-toxic Aβ$_{1-40}$ (left, grey) became highly toxic upon mixing with non-toxic Aβ$_{1-38}$ (left, black) and Aβ$_{1-43}$ (left, white) at a concentration of 10 μM. Toxicity of Aβ$_{1-42}$ (right, grey) is reduced upon addition of Aβ$_{1-38}$ (right, black) or Aβ$_{1-43}$ (right, white). Values are percent of cell viability ± SD (N=4),

buffer signal was normalized to 100 %. Statistical significance (unpaired 2-tailed t-test) compared to buffer control is indicated by *** P<0.0001, ** P<0.0005, and * P<0.005.
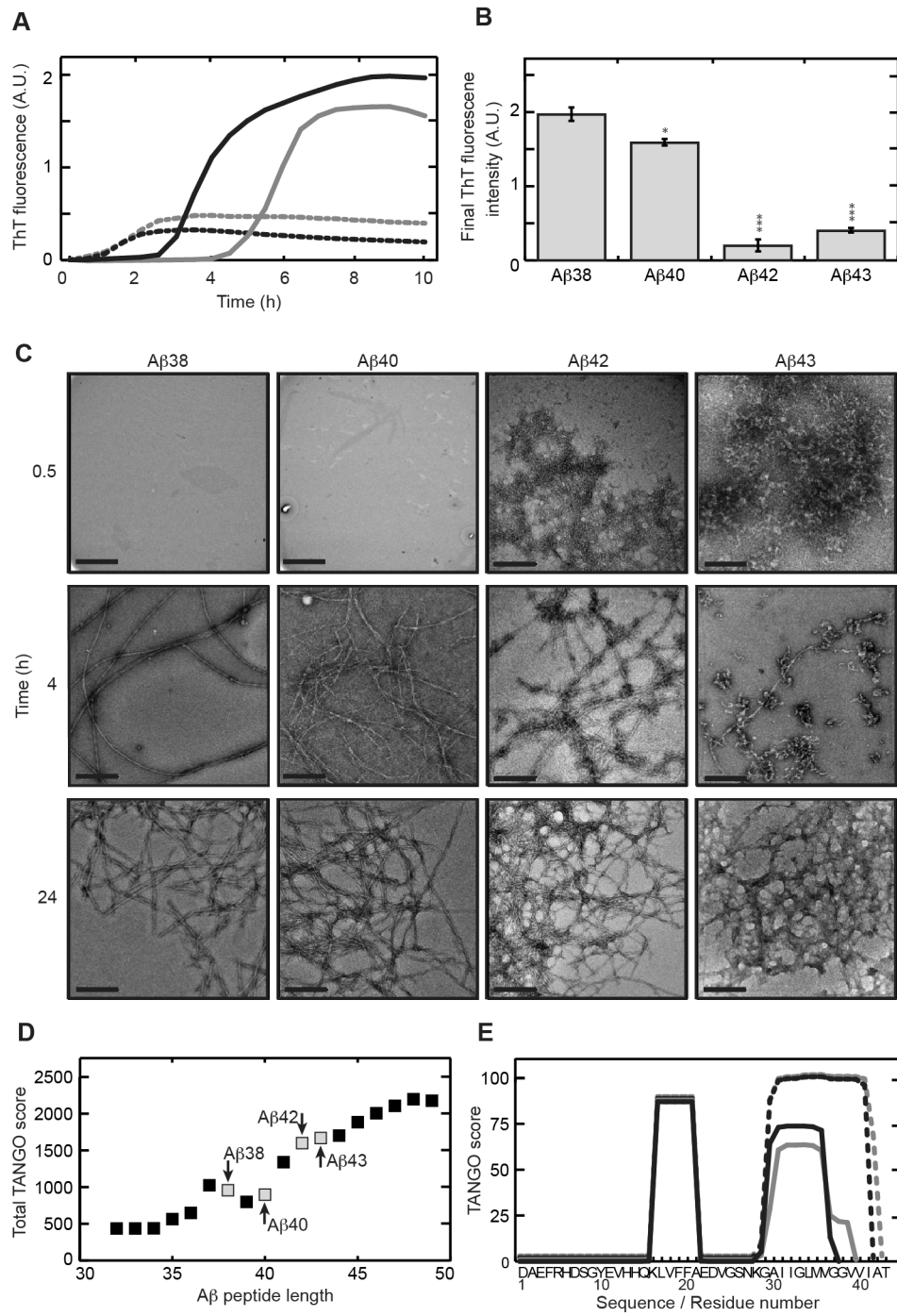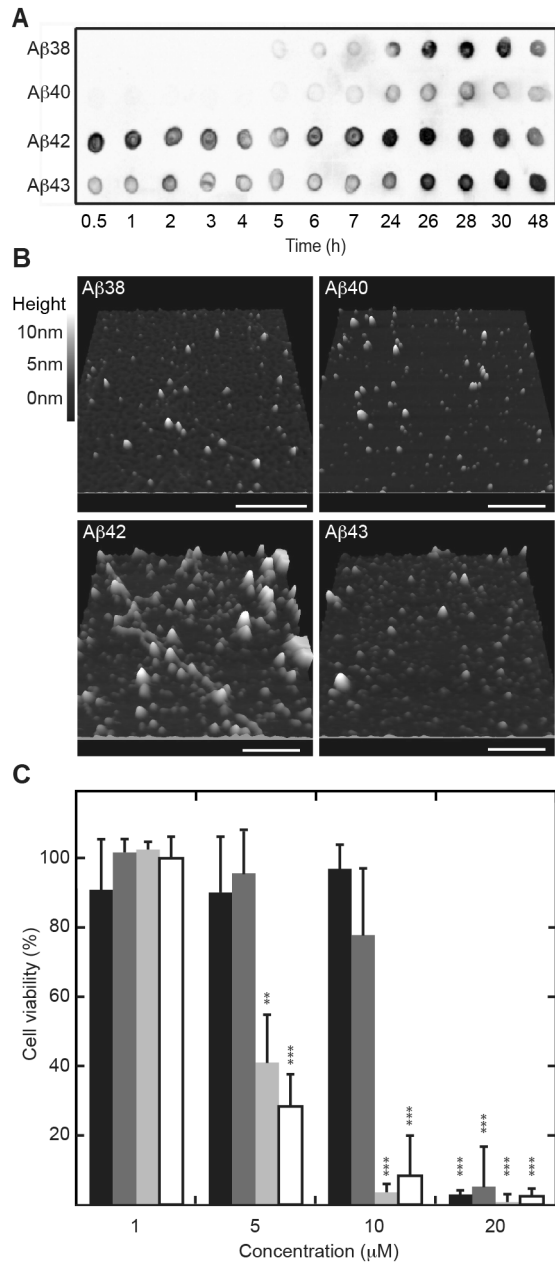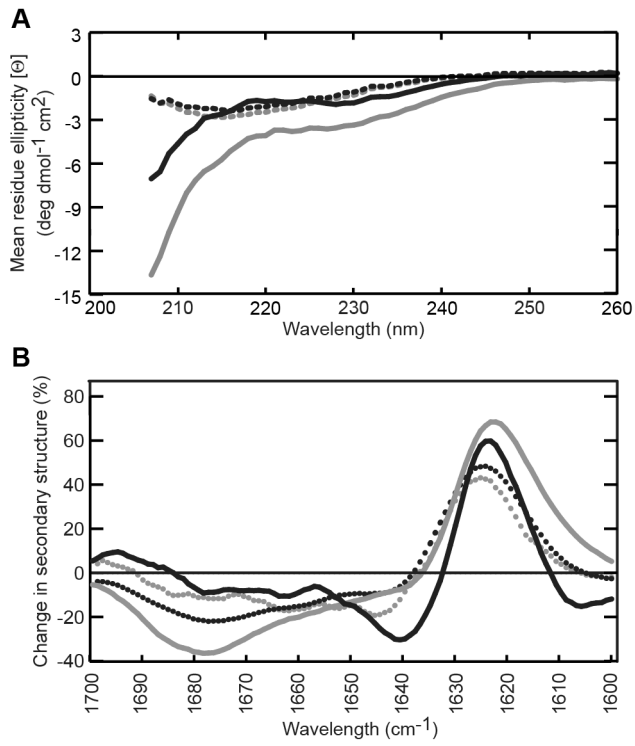
FIGURE 1

FIGURE 2

A

B

C

FIGURE 3

A

B

FIGURE 4

A

B

C

D

FIGURE 5

FIGURE 6

A

B

C

| | 9 : 1 Aβ40 : Aβ38 | 9 : 1 Aβ40 : Aβ43 | 9 : 1 Aβ42 : Aβ38 | 9 : 1 Aβ42 : Aβ43 |

D

E